Enhanced Infrared Absorption of C_{60} on Thin Evaporated Pd Island Films

TOSHIMASA WADAYAMA,* TAKAAKI OHTA, AND ARITADA HATTA
Department of Materials Science, Graduate School of Engineering, Tohoku University,
Aoba-yama 66-02, Sendai 980-8579, Japan

(Received 31 March 2005 and in revised form 22 July 2005)

Abstract. Infrared transmission spectra of C_{60} multilayers on thin Pd films deposited onto surface-oxidized Si(100) and hydrogen-terminated Si(111) substrates are reported. In both cases, the spectra in the 1500–1100 cm^{-1} region exhibited bands at 1444, 1429, and 1182 cm^{-1} due, respectively, to the A_g (2), T_{1u} (4), and T_{1u} (3) modes. The appearance of the A_g (2) mode, which is originally infrared inactive (Raman active), reveals electron transfer from the metal to chemisorbed C_{60}. Indeed, increasing the thickness of C_{60}, the A_g (2) mode intensity saturated more rapidly than the T_{1u} (4) and T_{1u} (3) modes. The originally infrared active T_{1u} (4) and T_{1u} (3) modes were enhanced in intensity depending upon the Pd thickness. Actually, while both substrates gave nearly the same magnitude of enhancement, the optimum Pd thickness was smaller on the hydrogen-terminated surface than on the surface-oxidized surface. On the other hand, the A_g (2) mode was less intense on the hydrogen-terminated surface than on the oxidized surface, suggestive of a shortage of chemisorbed C_{60} and thus pointing out the importance of the metal film morphology. Indeed, Pd films deposited on the two substrates gave rise to quite different AFM images. We also show that, regardless of the substrate, the A_g (2) mode is an order of magnitude smaller than for Ag deposition, though no remarkable intensity differences were observed with respect to the T_{1u} (4) and T_{1u} (3) modes.

INTRODUCTION

Very small metallic particles or clusters exhibit many interesting features that cannot be seen in bulk metals.[1] The features include aggregation, electron confinement (quantum size effects), extraordinary optical absorption, specific surface reactivity, etc. Colloidal particles of noble metals (e.g., Ag and Au) are known to show colors due to the excitation of plasma resonance. Ag bumps also exhibit a broad absorption band in the visible due to the transverse collective electron resonance in the bumps.[2] The colloidal particles and island films of such metals contribute to the surface-enhanced Raman scattering (SERS) from adsorbed molecules.[3,4] There is also evidence that the infrared absorption of molecules is enhanced on the evaporated thin films of Ag,[5–8] Cu,[9] Pt,[10] and Fe.[11] This is often referred to as surface enhanced infrared absorption (SEIRA).[8,12] Such enhancement also takes place on colloidal Ag particles when aggregated on solid surfaces.[13] The infrared absorption enhancements have mostly been explained in terms of surface enhanced electromagnetic fields caused by the excitation of the transverse collective electron resonances in the metal islands.[5–8]

Of particular interest is the application of the infrared absorption enhancement phenomenon to heterogeneous catalysts where small metallic particles are supported on fine oxide particles. Of special interest is the change of the catalytic activity of a particle with its dimensions. Although Au has been regarded as a catalytically inactive element, ultrafine Au particles serve as a good catalyst for oxidizing CO.[14] As is well known, Pd[15] is a catalytically important element for the control of automotive pollution since it is useful for reducing NO_x to N_2. Moreover, the oxidation of CO is activated on Pd

*Author to whom correspondence should be addressed.
E-mail: wadayamt@material.tohoku.ac.jp

particles dependent on their size. In this respect, the dependence of the metal particle size on the infrared absorption enhancement is worthy of investigation. Thus, it seemed to be important to examine the possibility of the infrared absorption enhancement on evaporated thin Pd films.

C_{60} is an attractive molecule because of its high degree of symmetry.[16] Further, the possibility of electron transfer from the metal substrate to C_{60} is interesting in the field of surface science. Actually, Manaila et al.[17] have shown a charge transfer for C_{60}/Cu based on Raman spectroscopy. The charge transfer has also been demonstrated more directly for a monolayer of C_{60} on several single crystalline metal substrates by using IR reflection absorption (IRRAS),[18-20] sum-frequency generation (SFGS),[18,19] and high-resolution electron energy loss (HREELS)[21,22] spectroscopies. Although many experimental approaches have been performed on C_{60} at the single crystalline metal surfaces, investigations at polycrystalline surfaces are limited.[23] This indeed was one of our motivations for the present work. We previously investigated the infrared absorption enhancement of C_{60} caused by evaporated Ag island films.[24,25] We focus in this paper on the infrared absorption of C_{60} in contact with evaporated Pd island films in the metal underlayer geometry. The dependence of Pd thickness on the absorption intensity is discussed in relation to the morphology of Pd films as judged by atomic force microscope (AFM) images.

EXPERIMENTAL

Palladium was deposited by electron-beam evaporation onto surface-oxidized Si(100) and hydrogen-terminated Si(111) substrates at room temperature in the MBE chamber[26] whose base pressure is 1×10^{-10} Torr, followed by depositing C_{60} in another chamber (1×10^{-9} Torr) from a resistively heated Ta boat. Each of the Pd-deposited wafers was transferred to the analysis chamber[26] to measure infrared absorption spectra. The thickness of Pd or C_{60} during deposition was monitored with a quartz oscillator. The infrared absorption spectra of C_{60} were taken at normal incidence in the 1500–1100 cm^{-1} region using an FT-IR spectrophotometer (Bomem, MB100) equipped with a liquid-nitrogen-cooled HgCdTe detector at an average of 400 scans. The spectral resolution was 1 cm^{-1}. Each of the spectra was ratioed against the spectrum recorded before C_{60} deposition.

The surface-oxidized substrates were prepared by dipping Si(100) wafers into an H_2O_2:HCl:H_2O = 1:1:5 (in volume) solution at 373 K for 30 min and further boiled in a 40% NH_4F aqueous solution for 1 h, followed by rinsing with distilled water.[27] The hydrogen-terminated substrates were prepared in the same way as above but without boiling in the NH_4F solution.

Morphologies of the deposited Pd films were inspected on an AFM (Digital Instruments Nanoscope E) under ambient conditions.

RESULTS AND DISCUSSION

(a) Infrared absorption of C_{60} on surface-oxidized Si(100) bare of Pd

The non-disturbed C_{60} molecule has a high symmetry (I_h) and has only four infrared active modes ($4T_{1u}$) and ten Raman active modes ($2A_g$+$8H_g$).[28] Actually, C_{60} deposited at room temperature on surface-oxidized Si(111) in the absence of Pd, exhibits two absorption bands, at 1429 and 1182 cm^{-1}, in the 1500–1100 cm^{-1} region, and their intensities increase in proportion to the thickness of C_{60}.[24,25] These were also confirmed for C_{60} deposited on Pd-free surface-oxidized Si(100) substrates. The infrared active bands at 1429 and 1182 cm^{-1} are due, respectively, to T_{1u} (4) and T_{1u} (3) modes.[29]

(b) Infrared absorption of C_{60} on Pd-deposited surface-oxidized Si(100)

Figure 1 depicts the absorption spectra of C_{60} in a thickness of 10 nm as a function of Pd thickness deposited on surface-oxidized Si(100) substrates. The most significant feature in Fig. 1 is the appearance of a new band at 1444 cm^{-1} in addition to the T_{1u} (4) and T_{1u} (3) modes at 1429 and 1182 cm^{-1}, respectively. It is clear from the band position that the new band is ascribed to the A_g (2) mode, which is originally infrared inactive but Raman-active.[30] The visibility of the A_g (2) mode can be explained by the chemisorption, which is accompanied by electron transfer from the Pd metal to the lowest unoccupied molecular orbital (LUMO) of the adsorbed C_{60}.[31] Further, the lower frequency shift of the A_g (2) mode from the corresponding Raman band can be explained by the chemisorption accompanied by charge transfer at the Pd surface. It is noted that the shift in position of the activated A_g (2) mode from the corresponding Raman band (1469 cm^{-1})[32,33] is 2 cm^{-1} smaller than that in the case of Ag,[24,25] indicating no significant difference between Pd and Ag with respect to the charge transfer. On the other hand, the T_{1u} (4) and T_{1u} (3) modes are, to begin with, infrared active and their intensities mostly bear reference to multilayers.

Additionally, the intensities of the three modes depend on Pd thickness, as more clearly shown in Fig. 2, where their intensities are plotted against the metal thickness. It is obvious that both the T_{1u} (4) and T_{1u} (3) modes are maximal in intensity at a Pd mass thickness of 5 nm, whereas the intensity of the A_g (2) mode decreases with increasing Pd thickness. The former fact probably means that the optimum Pd film structure was formed at 5 nm; perhaps the Pd film morphology could take part in the absorption intensities. Obviously, the latter fact cannot be explained in the same way. The intensity decrease of the A_g (2) mode with increasing Pd thickness signifies the decrease of suitable sites for

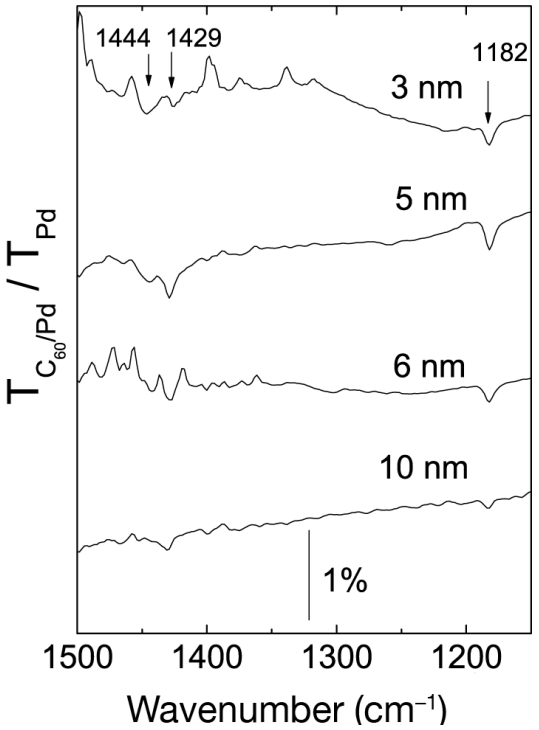

Fig. 1. Infrared absorption spectra of 10-nm-thick C_{60} as a function of the thickness of Pd deposited on surface-oxidized Si(100). The spectra are shifted vertically to avoid overlapping.

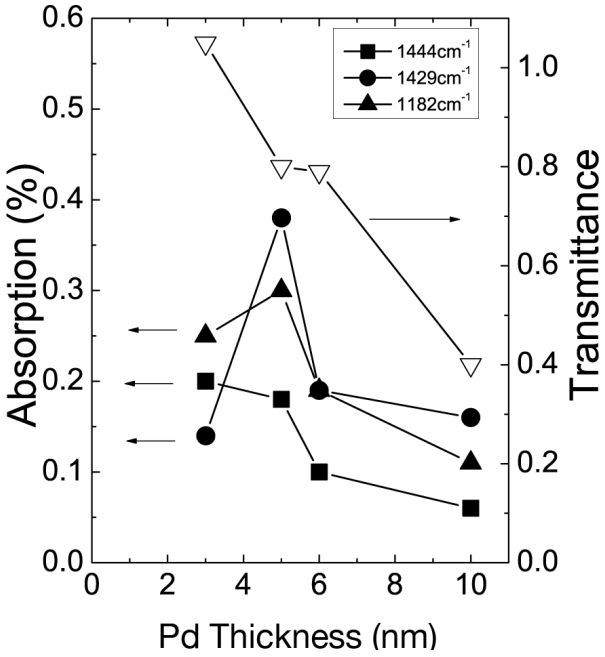

Fig. 2. Intensity changes of the A_g (2), T_{1u} (4), and T_{1u} (3) modes with increasing Pd thickness (from Fig. 1). The arrow-headed lines are a visual guide only. The infrared transmittance before C_{60} deposition also changes with Pd thickness.

C_{60} chemisorption. In this respect, it is likely that a microscopic film structure participates in the A_g (2) mode intensity. Also shown in Fig. 2 is the dependence of Pd thickness on the transmittance at 1150 cm^{-1} before C_{60} deposition. The transmittance change can be taken as a change in Pd film morphology and thus connecting itself with the observed C_{60} absorption intensities. Figure 2 reveals that the transmittance change breaks at a Pd thickness of 5 nm, for which the T_{1u} (4) and T_{1u} (3) modes are maximal in intensity. Similar features were also observed for colloidal Ag particles immobilized on Si(111) wafers, whereupon deposited organic molecules gave rise to maximum infrared absorption intensities at the break point of transmittance.[13] We shall later show some AFM images of Pd films deposited on the surface-oxidized Si(100) in relation to the Pd thickness dependence on the absorption intensities.

Figure 3 shows the absorption spectra for different thicknesses of C_{60} on 5-nm-thick Pd deposited on the surface-oxidized Si(100) substrate. It is immediately clear that the absorption intensities of the three modes are not commensurate with C_{60} coverage. The results of more quantitative intensity analysis are shown in Fig. 4, where the intensities of the A_g (2), T_{1u} (4), and T_{1u} (3) modes are plotted versus C_{60} thickness. Also shown in Fig. 4 is the T_{1u} (3) mode intensity observed in the absence of Pd (straight line). It should be noted that the intensity of the T_{1u} (3) mode in the absence of Pd was almost the same as that of the T_{1u} (4) mode. Thus, by reference to the straight line shown in Fig. 4 the intensities of the T_{1u} (4) and T_{1u} (3) modes are equally enhanced by the Pd film. It is also found that with increasing C_{60} thickness, the A_g (2) mode more rapidly saturates in intensity (i.e., at 5 nm) than the T_{1u} (4) and T_{1u} (3) modes. This result is explained by the fact that the A_g (2) mode arises from the first monolayer whereas T_{1u} (4) and T_{1u} (3) modes primarily concern the multilayers. The less rapid saturation of the two T_{1u} modes suggests that their enhancement is associated with an enhancement of the electromagnetic field generated at the metal surface. In Fig. 4 one may notice a little more increase of the T_{1u} (4) and T_{1u} (3) modes even when the C_{60} thickness exceeds 10 nm, due to Pd-unrelated absorption (normal absorption). In the present study, no attempt for estimating the roughness factor of the sample surface has been made, and therefore the enhancement factor of the IR absorptions caused by the adsorbed C_{60} cannot be evaluated definitively. Nevertheless, the absorption intensities of adsorbed C_{60} on the 5 nm-thick Pd/oxidized Si(100) surface are only 2–3 times larger than those on the oxidized

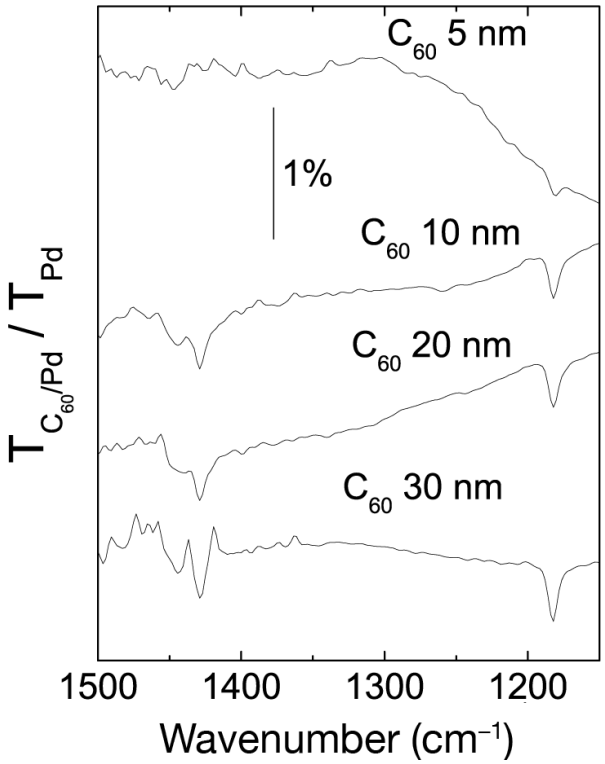

Fig. 3. The absorption spectra of C_{60} on 5-nm-thick Pd deposited as a function of C_{60} thickness deposited on surface-oxidized Si(100).

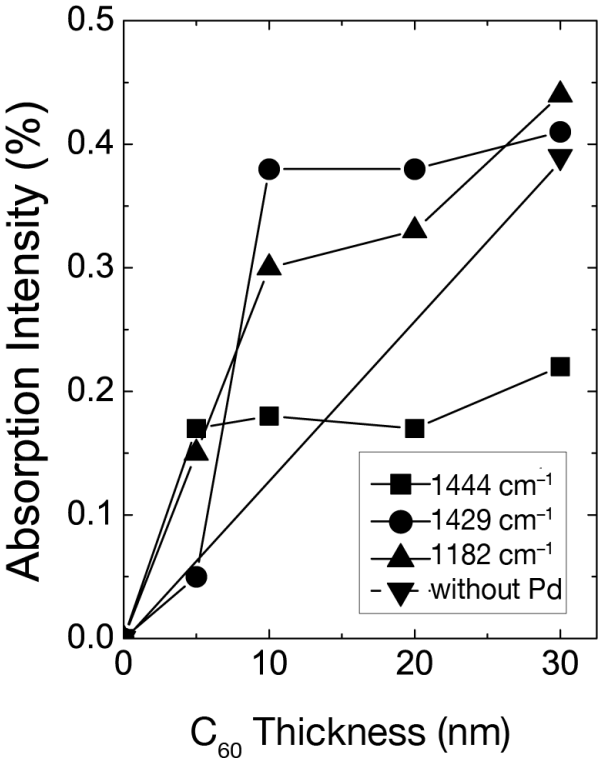

Fig. 4. Absorption intensities of the A_g (2), T_{1u} (4), and T_{1u} (3) modes versus C_{60} thickness on oxidized Si (100) (from Fig. 3). The intensity change of the T_{1u} (3) mode without Pd is also shown.

Si(100), indicating that the enhancement factor of the absorption is not so large for the deposited Pd islands.

(c) Infrared absorption of C_{60} on Pd-deposited hydrogen-terminated Si(111)

Figure 5 shows the absorption spectra of C_{60} in a thickness of 30 nm as a function of Pd thickness on the hydrogen-terminated Si(111) surface. In comparison to the case for Pd deposition on the oxidized Si(100) surface (Fig. 1), the optimum metal thickness to observe the T_{1u} (4) and T_{1u} (3) modes is smaller (2 nm). Moreover, each of the two T_{1u} modes is not noticeably different in intensity from that observed in Fig. 1 in spite of a larger C_{60} thickness (30 nm). In addition, the intensity of the A_g (2) mode is much smaller than that in the case of the oxidized surface. Most of these facts have to be explained by Pd film morphologies that are generally quite different from those on the oxidized surface, as shown later.

(d) Comparison of the Pd film morphologies on the surface-oxidized and hydrogen-terminated surfaces

We previously showed that the absorption intensities of the A_g (2), T_{1u} (4), and T_{1u} (3) modes differ on the two substrates, the features of which were explained implicitly in terms of the difference in Pd film morphology. We now show in Fig. 6 the AFM images of 3-, 5-, and 10-nm-thick Pd films deposited on surface-oxidized Si(100) wafers. A magnified image is also shown for each case in Fig. 6. In every case, the surface is sparsely dotted with large Pd bumps. We believe these bumps have almost nothing to do with the absorption enhancement, and of much more importance are the fine structures formed on the very substrate surface, the details of which are yet dependent on the metal thickness. Of particular interest is the formation of ridges for Pd deposition at 5 nm, for which the T_{1u} (4) and T_{1u} (3) modes are most intense (Fig. 2).

Figure 7 shows the AFM images of 2-, 5-, and 10-nm-thick Pd films on hydrogen-terminated Si(111) wafers. On that surface, the largest absorption intensities were obtained for 2-nm-thick Pd, as shown in Fig. 5. However, it should be noted that the intensities of the T_{1u} (4) and T_{1u} (3) modes were rather insensitive to the metal thickness even though the AFM image of the 2-nm Pd film is remarkably different from that of the 10-nm film, as clearly seen in Fig. 7. The reason for this

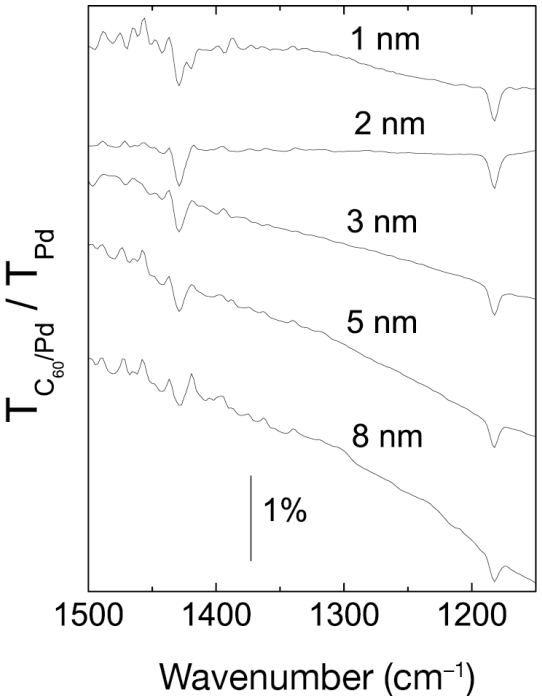

Fig. 5. Infrared absorption spectra of 30-nm-thick C_{60} as a function of the thickness of Pd on hydrogen-terminated Si(111).

is still unclear. Nevertheless, it is clear that the Pd morphologies are quite different from those on the oxidized surface. Also of importance is the fact that, in general, the intensity of the A_g (2) mode is much smaller than that observed with Pd deposition on the oxidized Si(100) surface. It seems difficult to explain this difference by the difference in the morphology of Pd films formed on the two substrates. Since the A_g (2) mode was activated via charge transfer at the very metal surface, it is very likely that a more microscopic surface structure takes part in the A_g (2) mode intensity. Thus, we consider that the terminated hydrogen exerted immense influence on the detailed Pd film structure and, in turn, the charge transfer. However, it should be noted that the intensity of the A_g (2) mode, as well as the intensities of the T_{1u} (4) and T_{1u} (3) modes, does not refer to all the chemisorbed C_{60} molecules, as far as the enhanced surface electromagnetic fields that indeed play a role in their absorption intensities.[9,33,34]

Now we compare the absorption features of C_{60} on the Pd films with those on surface-oxidized Si(100) and hydrogen-terminated Si(111) surfaces. The absorption spectra of 30-nm-thick C_{60} on 40-monolayer (ML)-thick Ag deposited on oxidized Si(100) and hydrogen-terminated Si(111) are shown in Fig. 8, together with the spectra for the same thickness of C_{60} on 2- and

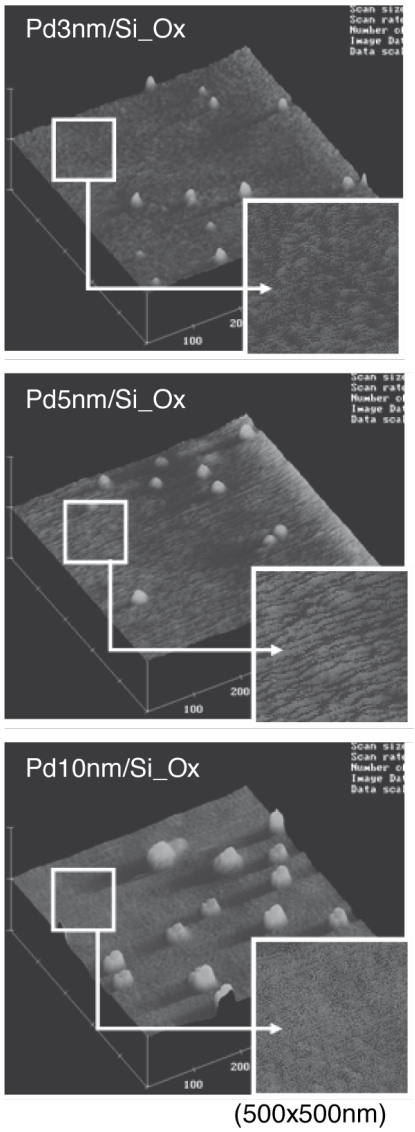

Fig. 6. AFM images of 3-, 5-, and 10-nm Pd films deposited on surface-oxidized Si (100)

5-nm-thick Pd films, respectively, deposited on the hydrogen-terminated and oxidized surfaces. It has already been shown that each of the Pd thickness values is optimum to observe the T_{1u} (4) and T_{1u} (3) modes. The Ag films were deposited by evaporation of the metal from a Knudsen cell in the MBE chamber.[26] The thicknesses of the Ag films were evaluated by referring to the deposition rate, as described previously.[24,25] It is clearly seen in Fig. 8 that the A_g (2) mode is less intense for the Ag deposition on the hydrogen-terminated surface than on the oxidized surface, as in the case of Pd. However, it must be emphasized that regardless of the substrate, the A_g (2) mode observed with Ag is an order of magnitude stronger than when Pd was deposited. In the case of Ag,

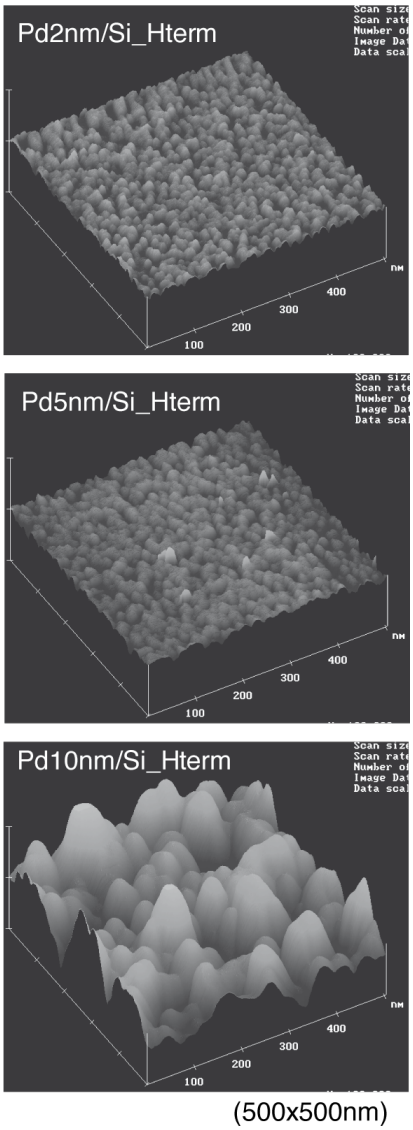

Fig. 7. AFM images of 2-, 5-, and 10-nm Pd films deposited on hydrogen-terminated Si(111)

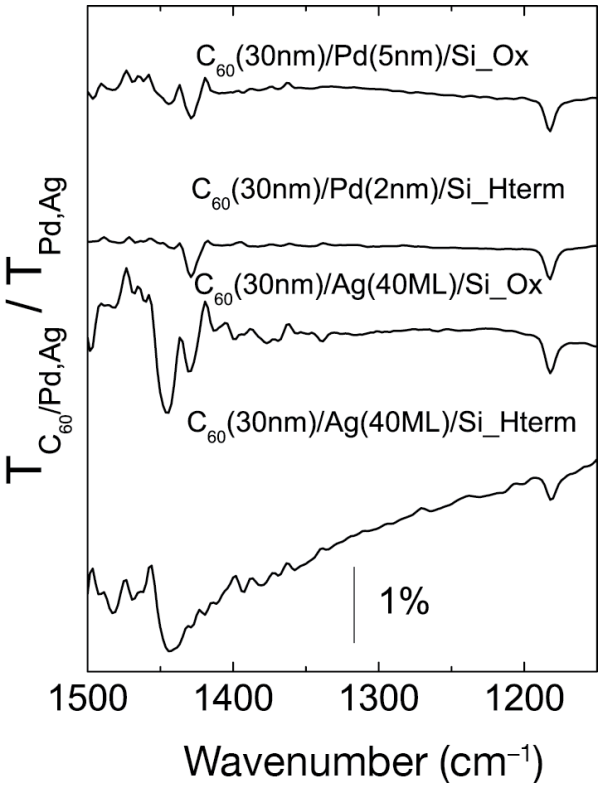

Fig. 8. The absorption spectra of 30-nm-thick C_{60} on 40 monolayer Ag deposited on surface-oxidized Si(100) and hydrogen-terminated Si(111), as compared with those of 30-nm C_{60} on the same substrates.

the A_g (2) mode is 5 times stronger than the T_{1u} (4) and T_{1u} (3) modes, independent of the substrate, unlike the case of Pd, where only for deposition on the oxidized surface the A_g (2) mode is comparable in intensity with the two T_{1u} modes. Thus, it can be deduced that C_{60} chemisorption onto the Pd metal deposited on the hydrogen-terminated surface is strongly hampered.

We again touch the charge transfer at the Pd/C_{60} interface as compared with that at the Ag/C_{60} interface. Since the originally infrared-inactive A_g (2) mode was activated only at that interface, its intensity should depend upon the population of adsorbed C_{60} molecules. It has been shown for C_{60} on single-crystalline Ag, Au, and Cu surfaces that the shift in position of the activated A_g (2) mode from its Raman band (1469 cm^{-1}) is proportional to the charge transferred from the metal to the adsorbed C_{60} (about 5 cm^{-1} per electron).[35] In our case, the peak of the Ag (2) mode activated by the Pd metal was observed at 1444 cm^{-1}, whereas the corresponding peak for Ag was positioned at 1442 cm^{-1}. This probably means that the charge transfer is a little smaller for the Pd than for the Ag. It is likely that the very little A_g (2) mode intensity for Pd deposition on the oxidized surface in comparison to the case for Ag deposition pertains at least in part to the smaller charge transfer. This is still more likely for the case of Pd deposition onto the hydrogen-terminated surface.

CONCLUSIONS

The results obtained in the present study are summarized as follows:

1. The IR absorption enhancement of the adsorbed C_{60} on the Pd thin films depends strongly upon the Pd islands morphologies.

2. IR activation of A_g (2) mode of the adsorbed C_{60} via charge transfer at the Pd/C_{60} interface is much less for Pd deposition on the hydrogen-terminated substrate than on the oxidized substrate.
3. The A_g (2) mode for Ag deposition enhanced more strongly in comparison to the case for Pd deposition although no remarkable difference was observed for the T_{1u} (4) and T_{1u} (3) modes.

Our infrared absorption measurements of C_{60} revealed that the originally infrared-active T_{1u} (4) and T_{1u} (3) modes are enhanced in intensity by underlying Pd films deposited on the surface-oxidized Si(100) and hydrogen-terminated Si(111) substrates. The intensities of these modes depend on the metal thickness and with increasing C_{60} thickness they saturate in a manner that can be qualitatively explained in terms of the enhancement of the surface electromagnetic fields. The metal thickness dependence on the enhancement was attributed to the Pd film morphologies. On the other hand, the intensity of the A_g (2) mode that was activated via charge transfer at the Pd/C_{60} interface was much less for Pd deposition on the hydrogen-terminated substrate than on the oxidized substrate. This fact suggests some significant influence of the terminated hydrogen upon nucleation and growth of Pd on the Si(111) surface, thereby limiting the direct contact of C_{60}. For Ag deposition on the oxidized and hydrogen-terminated substrates, the A_g (2) mode was much more enhanced in comparison to the case for Pd deposition, although no remarkable difference was observed for the T_{1u} (4) and T_{1u} (3) modes.

REFERENCES AND NOTES

(1) *Metal Clusters at Surfaces*; Meiwes–Broer, K.-H., Ed.; Springer: Berlin, 2000.
(2) Ritchie, G.; Burstein, E.; Stephens, R.B. *J. Opt. Soc. Am. B* **1985**, *2*, 544–551.
(3) *Surface Enhanced Raman Scattering*; Chang, R.K.; Furtak, T.E., Eds.; Plenum Press: New York, 1982.
(4) Otto, A. in *Light Scattering in Solids IV: Electronic Scattering, Spin Effects, SERS, and Morphic Effects*; Cardona, M.; Güntherodt, G., Eds.; Springer: Berlin, 1983.
(5) Hartstein, A.; Kirtley, J.R.; Tsang, J.C. *Phys. Rev. Lett.* **1980**, *45*, 201–204.
(6) Hatta, A.; Ohshima, T.; Suëtaka, W. *Appl. Phys. A* **1982**, *29*, 71–75.
(7) Hatta, A.; Suzuki, Y.; Suëtaka, W. *Appl. Phys. A* **1984**, *35*, 135–140.
(8) Osawa, M. *Bull. Chem. Soc. Jpn.* **1997**, *70*, 2861–2880.
(9) Seki, H.; Takada, M.; Tanabe, T.; Wadayama, T.; Hatta, A. *Surf. Sci.* **2002**, *506*, 23–32.
(10) Bjerke, A.E.; Griffiths, P.R. *Appl. Spectrosc.* **2002**, *56*, 1275–1280.
(11) Priebe, A.; Fahsold, G.; Geyer, W.; Pucci, A. *Surf. Sci.* **2002**, *502–503*, 388–393.
(12) Aroca, R.F.; Ross, D.J.; Domingo, C.; *Appl. Spectrosc.* **2004**, *58*, 324A–338A.
(13) Wadayama, T.; Yano, H.; Sasaki, Y.; Takahashi, J.; Hatta, A. *Mater. Trans.* **2004**, *45*, 86–91.
(14) Haruta, M. *Catal. Today* **1997**, *36*, 153–166.
(15) Dumas, P.; Suhren, M.; Chabal, Y.T.; Hirschmal, C.J.; Williams, G.P. *Surf. Sci.* **1997**, *371*, 200–212.
(16) Kuzmany, H.; Winkler, R.; Pichler, T. *J. Phys.: Condens. Matter* **1995**, *7*, 6601–6624.
(17) Manaila, R.; Belu-Marian, A.; Macovei, D.; Brehm, G.; Marian, D.T.; Baaltog, I. *J. Raman Spectrosc.* **1999**, *30*, 1019–1025.
(18) Caudano, Y.; Premans, A.; Thiry, P.A.; Dumas, P.; Tadjeddine, A. *Surf. Sci.* **1996**, *368*, 337–341.
(19) Premans, A.; Caudano, Y.; Thiry, P.A.; Dumas, P.; Zhang, W.Q.; Rille, A.L.; Tadjeddine, A. *Phys. Rev. Lett.* **1997**, *78*, 2999–3002.
(20) Dumas, P.; Hein, M.; Otto, A.; Persson, B.N.J.; Rudolf, P.; Raval, R.; Williams, G.P. *Surf. Sci.* **1999**, *433–435*, 797–805.
(21) Silien, C.; Caudano, Y.; Peremans, A.; Thiry, P.A. *Appl. Surf. Sci.* **2000**, *162–163*, 445–451.
(22) He, H.; Swami, N.; Koel, B.E. *Thin Solid Films* **1999**, *348*, 30–37.
(23) Goldni, A.; Paolucci, G. *Surf. Sci.* **1999**, *437*, 353–361.
(24) Wadayama, T.; Takada, M.; Sugiyama, K.; Hatta, A. *Phys. Rev. B* **2002**, *66*, 193401 (1)–(4).
(25) Wadayama, M.; Aoshima, K.; Kawano, S.; Hatta, A. *Appl. Spectrosc.* **2004**, *58*, 299–303.
(26) Tanabe, T.; Shibahara, T.; Buckmaster, R.; Ishibashi, T.; Wadayama, T.; Hatta, A. *Surf. Sci.* **2000**, 466, 1–10.
(27) Jacob, P.; Chabal, Y.J.; Kuhnke, K.; Cristman, S.B. *Surf. Sci.* **1994**, *302*, 49–56.
(28) Weeks, D.-E.; Harter, W.G. *J. Chem. Phys.* **1989**, *90*, 4744–4771.
(29) Bohnen, K.-P.: Heid, R.; Ho, K.-M.; Chan, C.T. *Phys. Rev. B* **1995**, *51*, 5805–5813.
(30) Chase, B.; Herron, N.; Holler, E. *J. Phys. Chem.* **1992**, 96, 4262–4266.
(31) Johnson, E.; Aroca, R. *J. Phys. Chem.* **1995**, 99, 9325–9330.
(32) Wang, K.-A.; Rao, A.M.; Eklund, P.C.; Dresselhaus, M.S.; Dresselhaus, G. *Phys. Rev. B* **1993**, *48*, 11375–11380.
(33) Zhou, P.; Wang, K.; Wang, Y.; Eklund, P.C.; Dresselhaus, M.S.; Dresselhaus, G.; Jishi, R.A. *Phys. Rev. B* **1992**, *46*, 2595–2605.
(34) (a) Suzuki, Y.; Seki, H.; Inamura, T.; Tanabe, T.; Wadayama, T.; Hatta, A. *Surf. Sci.* **1999**, *427–428*, 136–140. (b) Suzuki, Y.; Seki, H.; Inamura, T.; Tanabe, T.; Wadayama, T.; Hatta, A. *Surf. Sci.* **1999**, *433–435*, 261–266.
(35) Rudolf, P.; Raval, R.; Dumas, P.; Williams, G.P. *Appl. Phys. A* **2002**, *75*, 147–153.